

Synthesis and Electrochemical Properties of Vanadium Pentoxide Nanotube Arrays

Ying Wang,[†] Katsunori Takahashi,^{†,‡} Huamei Shang,[†] and Guozhong Cao^{*,†}

Materials Science and Engineering, University of Washington, 302 Roberts Hall, Box 352120, Seattle, Washington 98195, and Steel Research Laboratory, JFE Steel Corporation, Kawasaki-cho, Chuo-ku, Chiba 260-0835, Japan

Received: December 15, 2004; In Final Form: January 21, 2005

Nanotube arrays of amorphous vanadium pentoxide (V_2O_5) were synthesized via template-based electrodeposition, and its electrochemical properties were investigated for Li-ion intercalation applications. The nanotubes have a length of 10 μm , outer diameter of 200 nm and inner diameter of 100 nm. Electrochemical analyses demonstrate that the V_2O_5 nanotube array delivers a high initial capacity of 300 mAh/g, about twice that of the electrochemically prepared V_2O_5 film. Although the V_2O_5 nanotube array shows a more drastic degradation than the film under electrochemical redox cycles, the nanotube array reaches a stabilized capacity of 160 mAh/g, which remains about 1.3 times the stabilized capacity of the film.

Introduction

Vanadium pentoxide (V_2O_5) has attracted considerable attention as a Li-ion intercalation material due to its layered structure.^{1,2} Lithium ions can be intercalated and deintercalated between the adjacent layers of V_2O_5 . As a result, electrical energy is stored in the V_2O_5 electrode during intercalation, and energy is released during deintercalation. Hence V_2O_5 finds wide applications in energy storage devices such as lithium batteries^{3,4} and electrochemical supercapacitors.^{5,6} However, the intercalation capacity and charge/discharge rate of V_2O_5 are limited by the moderate electrical conductivity (10^{-2} – 10^{-3} S/cm)^{7,8} of V_2O_5 and the low diffusion coefficient of Li ions (10^{-12} – 10^{-13} cm²/s)^{9,10} in the V_2O_5 matrix. To overcome these disadvantages, increasing the surface area and shortening the diffusion distance of the intercalation electrode play important roles. Nanostructured materials possess large surface area and short diffusion paths, and thus offer promises to achieve significantly enhanced intercalation capacity.

Ordered arrays of nanorods, nanotubes, or core–shell nanocables are one of the most promising nanostructures for Li⁺-intercalation applications. Martin et al. investigated the electrochemical properties of V_2O_5 nanorod arrays made by depositing vanadium pentoxide sol within pores of polycarbonate (PC) membranes, and reported that nanorod arrays achieved four times the capacity of a thin-film electrode at high discharge rate.¹¹ We recently fabricated single-crystal V_2O_5 nanorod arrays by using electrochemical deposition, surface condensation induced by a change of local pH as a result of H₂O electrolysis, and sol–gel electrophoretic deposition, combined with template growth methods.^{12,13} The single-crystal V_2O_5 nanorod-array electrode delivers five times higher capacity than sol–gel derived films at a current density of 0.7 A/g.¹³ We have also

prepared Ni– $V_2O_5 \cdot nH_2O$ nanocable arrays and demonstrated that at a current density of 1.6 A/g, the Li⁺-intercalation capacity of Ni– $V_2O_5 \cdot nH_2O$ nanocable array is approximately 10 times higher than that of single-crystal V_2O_5 nanorod array and 20 times higher than that of sol–gel-derived V_2O_5 film.¹⁴ These results confirm that the specific surface area of electrode is important since the redox or intercalation reactions occur at and near the electrode interface with electrolyte, hence nanostructured electrode is effective for Li-ion intercalation processes.

Compared to nanorods, nanotubes possess several different areas of contact, i.e., the inner and outer wall surfaces as well as the open ends. In principle, nanotube arrays have even larger surface area than nanorod arrays. In addition, the tubes can operate as electrolyte-filled channels for faster transport of the ions to the intercalation sites. Mixed-valent vanadium(+4, +5) oxide nanotubes (VO_x NTs) have been obtained in high yield by treating a vanadium(V) oxide precursor with an amine that has long alkyl chains, followed by hydrolyzation and hydrothermal reaction.¹⁵ The amine functions as a molecular, structural directing template and the resulted VO_x NT has a scroll-like morphology. This material opens new perspectives for Li⁺-intercalation applications and has been widely studied recently. Several research groups have measured its discharge capacities up to 200 mAh/g,^{16,17} though its morphological flexibility leads to rapid degradation of capacity.¹⁸

Template-based electrodeposition is a simple and efficient route for producing oxidic nanorods and nanotubes.¹⁹ Furthermore, the template-based electrodeposition method has the advantage of fabricating a well-ordered ensemble of nanorods or nanotubes standing up from the substrate surface which promise large surface area, while nanorods or nanotubes synthesized by other methods such as solvothermal processes are scattered and possess less surface area when they are collected and pressed into pellets for electrode use. It has been found that amorphous or low-crystalline V_2O_5 has higher intercalation capacity than crystalline V_2O_5 .^{20,21} In this paper we have prepared nanotube arrays of amorphous V_2O_5 through

* Corresponding author. E-mail: gzcao@u.washington.edu; Fax: 206-543-3100.

[†] University of Washington.

[‡] JFE Steel Corporation.

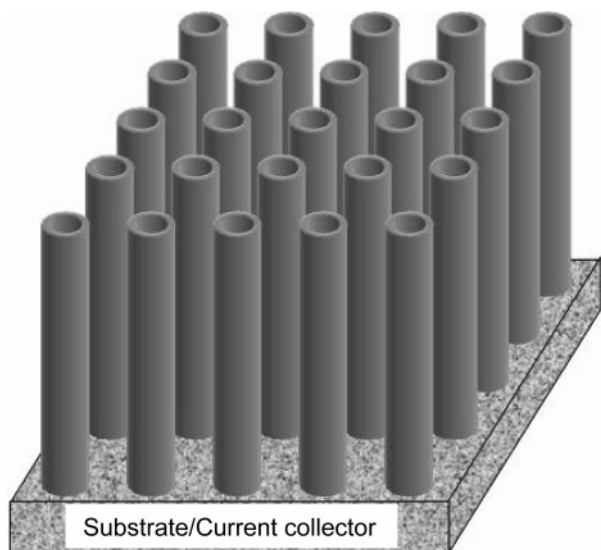


Figure 1. Schematic illustration of V_2O_5 nanotube array.

the template-based electrodeposition. Figure 1 shows a schematic illustrating the V_2O_5 nanotube array as the Li^+ -intercalation electrode. The amorphous V_2O_5 nanotube arrays achieved a capacity of 300 mAh/g, which is higher than the maximal capacity of crystalline V_2O_5 nanorod arrays (up to one equivalent of Li^+ per mole of V_2O_5 , i.e., 150 mAh/g) reported by Martin's group¹¹ and our group¹³ previously. Such improvement in the maximum capacity is ascribed to the larger surface area and amorphous nature of V_2O_5 nanotubes. The amorphous V_2O_5 nanotube arrays also possessed about twice the capacity of the amorphous V_2O_5 film made from the same electrodeposition process, which is ascribed to the larger surface area of nanotube arrays. Cyclic performances of both amorphous V_2O_5 nanotube arrays and amorphous V_2O_5 films are further discussed in this report.

Experimental Section

The chemicals used in synthesizing the solution were $VOSO_4 \cdot nH_2O$ (Alfa Aesar) and H_2SO_4 (96.5%, Fisher). The $VOSO_4$ solution was prepared by dissolving $VOSO_4 \cdot nH_2O$ into deionized water together with H_2SO_4 in a concentration of 0.1 M $VOSO_4$ and 0.03 M H_2SO_4 . Such a solution is blue in color and has a pH of 1.7. The primary vanadium ionic clusters in the solution are VO^{2+} .

The templates used for this study were radiation track-etched hydrophilic PC membrane (Millipore, Bedford, MA) with pore diameters of 200 nm and thickness of 10 μm . An aluminum sheet of 9 mm in diameter was used as the working electrode and placed beneath the template, and a platinum mesh was used as the counter electrode. The distance between the two electrodes was kept at 25 mm. For the growth of nanotube arrays, direct electrochemical reactions at the electrode interface with the electrolyte are necessary. To ensure a good electrical contact between the template and electrode, the back of the membrane template was first sputter-coated with Au-Pd alloy before attaching to the working electrode. A detailed description of the deposition setup can be found in our recent publications.^{22,23} The applied electric voltage ranges from 1.5 to 2 V, and the deposition time lasted up to 2 h. Upon the completion of deposition, the sample was dried at 110 $^{\circ}C$ for 6 h and was then attached to ITO substrate with silver paste (Ted Pella Inc.). The as-prepared sample on ITO substrate was dried at 110 $^{\circ}C$ for another 6 h and was immersed in methylene chloride to

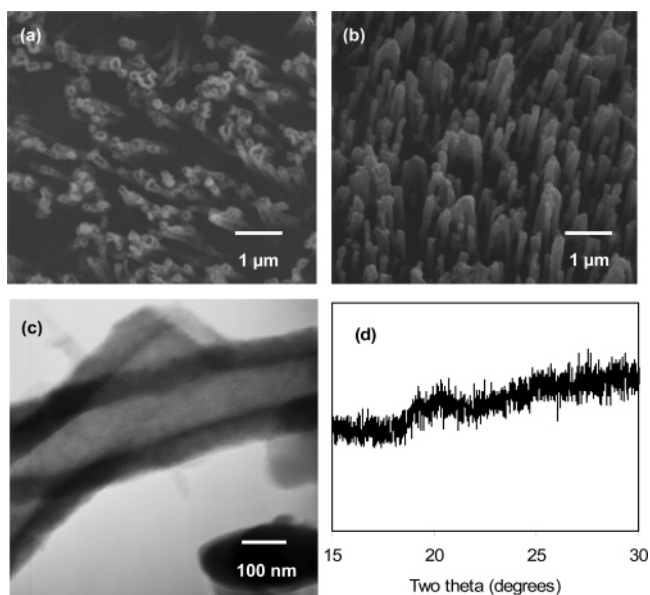


Figure 2. SEM images of (a) top view and (b) side view of V_2O_5 nanotubes electrochemically deposited within 200-nm-dia pores of PC membrane. (c) TEM micrographs of isolated V_2O_5 nanotubes. (d) XRD pattern of the electrochemically prepared V_2O_5 film on Au electrode.

dissolve away PC membrane, resulting in an ensemble of V_2O_5 nanotubes attached on the ITO substrate.

Scanning electron microscopy (SEM, JEOL JSM-5200) was used to characterize the morphology of nanotube arrays. Transmission electron microscopy (TEM) images were recorded with Phillips EM420 at accelerating voltage of 120 kV. The V_2O_5 film prepared under the same condition via electrochemical deposition from $VOSO_4$ solution was characterized by X-ray diffractometry (XRD, Philips PW 1820).

Electrochemical properties of nanotube arrays were investigated using a three-electrode cell. A 1-M $LiClO_4$ solution in propylene carbonate was used as electrolyte; a platinum mesh was used as the counter electrode and $Ag/AgNO_3$ as the reference electrode. Cyclic voltammetry and chronopotentiometry were carried out by a potentiostat/galvanostat (CH Instruments, model 605B) between the potential limits of -1.6 and 0.4 V versus Ag/Ag^+ .

Results and Discussion

Figure 2 shows SEM images of (a) top view and (b) side view of V_2O_5 nanotube array grown within the pores of PC membrane after the membrane is dissolved away in methylene chloride. These nanotubes stand apart from each other and project straight up from the substrate surface, with a length of 10 μm (image not shown). As can be seen from the TEM images in Figure 2c, the outer diameter of nanotube is about 200 nm and the inner diameter of nanotube is about 100 nm. No electron diffraction pattern in TEM was observed, which suggests the amorphous nature of these nanotubes. XRD analysis of nanotube arrays shows its amorphous state as well. However, such XRD result may be because the low crystallinity and the small amount of V_2O_5 of one nanotube array is beyond XRD detection limit. We then prepared V_2O_5 film through electrochemical deposition from the same $VOSO_4$ solution and under the same deposition condition. Figure 2d shows XRD pattern of V_2O_5 film deposited on the Au electrode, which confirms its amorphous nature. The constant potential electrolysis from $VOSO_4$ has been reported by Sato et al. to produce V_2O_5 .²⁴ Furthermore, in our case of film deposition, the resultant film is greenish in color, indicating

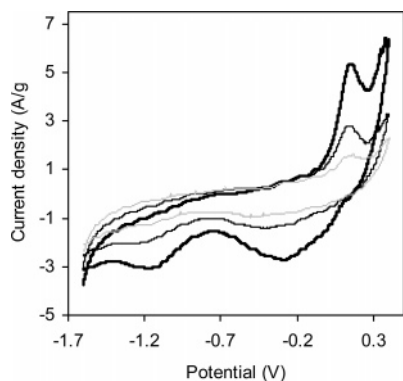
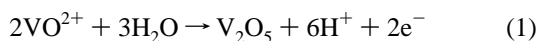


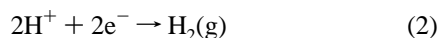
Figure 3. Cyclic voltammograms of V_2O_5 nanotube array in a potential range between -1.6 V and 0.4 V vs. Ag/Ag^+ and under the scan rate of 10 mV/s. Thick solid line: the first cycle; thin solid line: the second cycle; dotted line: the third cycle.

that our deposition product is V_2O_5 instead of mixed-valent $V(+4, +5)$ oxides, since mix-valent vanadium oxides are generally black.

The possible mechanism of the nanotube growth is discussed as follows. A very thin coating of $Au-Pd$ alloy on the PC membrane results in coating of metal on the edges of pores, leading to high current density on these edges, where electrochemical reaction and deposition are initiated. On the edges of pores, the ionic cluster, VO^{2+} , is oxidized to deposit V_2O_5 through the following reaction:



Simultaneously a reduction reaction occurs at the counter electrode:



It has been documented in literature that there are anionic sites on the pore walls of the PC membrane, and conductive polymer nanotubes have been synthesized because the polymers are cationic.²⁵ Similarly, cations such as VO^{2+} preferentially adhere to the wall because of the electrostatic attraction and undergo electrochemical reactions. In the case of growing conductive polymer nanostructures through template-based electrochemical-deposition, thin-walled tubes, thick-walled tubes, or solid rods can be formed, respectively, by controlling polymerization time.¹⁸ Similarly, for the template-based growth of V_2O_5 from $VOSO_4$ solution, lower voltage and shorter time of deposition lead to nanotube formation, while higher voltage and longer deposition result in nanorods, indicated by the present work on V_2O_5 nanotubes and our previous report on V_2O_5 nanorods.¹³

Figure 3 shows the first three voltammograms of the V_2O_5 nanotube arrays in the potential range between -1.6 and 0.4 V vs Ag/Ag^+ and using a scan rate of 10 mV/s. The cyclic voltammogram (CV) of the nanotube arrays shows cathodic peaks at -0.3 V and -1.2 V, corresponding to Li^+ intercalation, and anodic oxidation peaks at 0.17 and 0.4 V, which are attributed to Li^+ extraction. It can be seen from Figure 3 that these cathodic and anodic peaks become more flattened and the area of the voltammogram shrinks under the electrochemical redox cycles, indicating the material loses some electroactivity. The degradation may be either ascribed to the electrochemically deposited V_2O_5 itself or due to the fragile structure of nanotubes. Being consistent with cyclic voltammograms, chronopotentiograms (CP) have shown that nanotube arrays exhibit degradation in electrochemical performance as well, and the quantitative

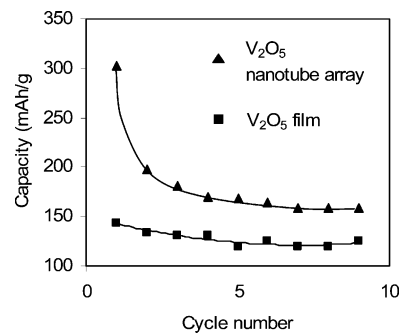


Figure 4. Dependence of the discharge capacity on the cycle number obtained from chronopotentiometric measurements at a 0.4 V to -1.5 V cutoff voltage vs. Ag/Ag^+ .

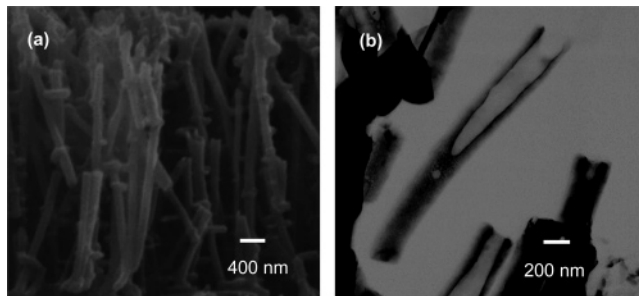


Figure 5. (a) SEM and (b) TEM image of V_2O_5 nanotubes after electrochemical measurements.

results of capacities calculated from chronopotentiometric measurements are discussed as follows.

Figure 4 illustrates the dependence of discharge capacity on cycle number for both nanotube array and film prepared from the electrochemical deposition method. The capacity of nanotube array is calculated based on the outer diameter of 200 nm, the inner diameter of 100 nm, length of $10 \mu m$, and the density of 2.87 g/cm³.²⁶ The V_2O_5 nanotube arrays demonstrate an initial high capacity of 300 mAh/g, about twice the initial capacity of 140 mAh/g from the V_2O_5 film. Such enhancement of capacity is due to the large surface area and short diffusion distances offered by the nanotube array. However, the capacity of the nanotube array decayed to 200 mAh/g in the second cycle and 180 mAh/g in the third one. The degradation is slower in the further cycles and finally reaches a stabilized capacity of 160 mAh/g after the sixth cycle, which is about 30% higher than the stabilized capacity of V_2O_5 film. Our other work on the electrochemical intercalation properties of V_2O_5 films up to 50 cycles revealed little or no further degradation after initial $5-10$ cycles.²⁷ The initial degradation of V_2O_5 film suggests V_2O_5 itself prepared from electrochemical deposition has some drawback and suffers a slight loss of electroactivity during cycling. However, nanotube arrays show a more drastic decay of initial performance compared to the film during cycling, possibly due to the morphological flexibility and fragility of nanotubes, which has been speculated in the literature as well.¹⁸ Our further SEM and TEM analyses of nanotube arrays after electrochemical measurements, up to 10 cycles, also indicated the occurrence of partial fracture of nanotubes after redox cycles, as shown in Figure 5. Such structural breakdown may well explain the degradation of electrochemical intercalation properties. It seems that such structural breakdown occurred only in the initial cycles, whereas there was little or no further structural breakdown afterward. The systematic study on long-term cyclability of V_2O_5 and its relationship with structural stability is currently under way and will be reported and discussed later on.

Conclusions

We have demonstrated a simple and efficient method for the preparation of nanotube arrays of amorphous V_2O_5 by combining template synthesis and electrochemical deposition. Investigation of its electrochemical properties shows the nanotube array possesses a high Li^+ -intercalation capacity of 300 mAh/g, about twice that of the electrochemically prepared V_2O_5 film. Although the capacities of both the nanotube array and the film decrease during cycling, they reach stabilized capacities within 10 cycles. The stabilized capacity of the nanotube is approximately 160 mAh/g and remains 30% higher than the stabilized capacity of the film. The initial high capacity of the nanotube is obviously ascribed to the large surface area and short diffusion distances provided by the nanostructure. However, the flexibility and fragility of the nanotube array may also lead to the initial degradation in electrochemical performance.

Acknowledgment. Y.W. would like to acknowledge the financial support from the Ford company fellowship, and H.M.S. acknowledges the graduate fellowship from the Joint Institute of Nanoscience and Nanotechnology, University of Washington and Pacific Northwest National Laboratories.

References and Notes

- (1) Bachmann, H. G.; Ahmend, F. R.; Barnes, W. H. Z. *Kristallogr.* **1961**, *115*, 110.
- (2) Whittingham, M. S. *J. Electrochem. Soc.* **1976**, *123*, 315.
- (3) Park, H. K.; Smryl, W. H.; Ward, M. D. *J. Electrochem. Soc.* **1995**, *142*, 15.
- (4) Swider-Lyons, K. E.; Love, C. T.; Rolison, D. R. *Solid State Ionics* **2002**, *152–153*, 99.
- (5) Portion E.; Salle, A. L. G. A.; Verbaere, A.; Piffard, Y.; Guyomard, D. *Electrochem. Acta* **1999**, *45*, 197.
- (6) Shimizu, A.; Tsumura, T.; Inagaki, M. *Solid State Ionics* **1993**, *63–65*, 479.
- (7) Coustier, F.; Hill, J.; Owens, B. B.; Passerini, S.; Smryl, W. H. *J. Electrochem. Soc.* **1999**, *146*, 1355.
- (8) Livage, J. *Chem. Mater.* **1991**, *3*, 578.
- (9) Portiron, E.; Salle, A. L.; Verbaere, A.; Piffard, Y.; Guyomard, D. *Electrochim. Acta* **1999**, *45*, 197.
- (10) Lantelme, F.; Mantoux, A.; Groult, H.; Lincot, D. *J. Electrochem. Soc.* **2003**, *150*, A1202.
- (11) Patrissi, C. J.; Martin, C. R. *J. Electrochem. Soc.* **1999**, *146*, 3176.
- (12) Takahashi, K.; Limmer, S. J.; Wang, Y.; Cao, G. Z. *Jpn. J. Appl. Phys.* **2005**, *44*, 662.
- (13) Takahashi, K.; Limmer, S. J.; Wang, Y.; Cao, G. Z. *J. Phys. Chem. B* **2004**, *108*, 9795.
- (14) Takahashi, K.; Wang, Y.; Cao, G. Z. *J. Phys. Chem. B* **2005**, *109*, 48.
- (15) Spahr, M. E.; Bitterli, P.; Nesper, R.; Müller, M.; Krumeich, F.; Nissen, H. U. *Angew. Chem., Int. Ed.* **1998**, *37*, 1263.
- (16) Spahr, M. E.; Stoschitzki-Bitterli, P.; Nesper, R.; Haas, O.; Novák, P. *J. Electrochem. Soc.* **1999**, *146*, 2780.
- (17) Doble, A.; Ngala, K.; Yang, S.; Zavalij, P. Y.; Whittingham, M. S. *Chem. Mater.* **2001**, *13*, 4382.
- (18) Patzke, G. R.; Krumeich, F.; Nesper, R. *Angew. Chem., Int. Ed.* **2002**, *41*, 2446.
- (19) Hulteen, J. C.; Martin, C. R. *J. Mater. Chem.* **1997**, *7*, 1075.
- (20) Coustier, F.; Passerini, S.; Smryl, W. H. *Solid State Ionics* **1997**, *100*, 247.
- (21) Scarmionio, J.; Talledo, A.; Anderson, A. A.; Passerini, S.; Decker, F. *Electrochim. Acta* **1993**, *38*, 1637.
- (22) Limmer, S. J.; Cao, G. Z. *Adv. Mater.* **2003**, *15*, 427.
- (23) Limmer, S. J.; Chou, T. P.; Cao, G. Z. *J. Mater. Sci.* **2004**, *39*, 895.
- (24) Sato, Y.; Nomura, T.; Tanaka, H.; Kobayakawa, K. *J. Electrochem. Soc.* **1991**, *138*, L37.
- (25) Martin, C. R. *Adv. Mater.* **1991**, *3*, 457.
- (26) Liu, Y. J.; Cowen, J. A.; Kaplan, T. A.; DeGroot, D. C.; Schindler, J.; Kannewurf, C. R.; Kanatzidis, M. G. *Chem. Mater.* **1995**, *7*, 1616.
- (27) Lee, K. H.; Cao, G. Z., unpublished work.